J Musculoskelet Neuronal Interact 2015; 15(1):42-52

Original Article

Hylonome

Comparison between quantitative X-ray imaging, dual energy X-ray absorptiometry and microCT in the assessment of bone mineral density in disuse-induced bone loss

G. Mabilleau[1,2], A. Mieczkowska[1], H. Libouban[1], Y. Simon[3], M. Audran[1,3], D. Chappard[1,2]

[1]GEROM Groupe d'Etudes et Remodelage Osseux et bioMatériaux, IRIS-IBS Institut de Biologie en Santé, LUNAM Université, CHU d'Angers, 49933 ANGERS Cedex - FRANCE; [2]SCIAM, Service Commun d'Imagerie et Analyses Microscopiques, IRIS-IBS Institut de Biologie en Santé, CHU d'Angers, LUNAM Université, 49933 ANGERS Cedex - FRANCE; [3]Service de Rhumatologie, CHU d'Angers, 49933 ANGERS Cedex - FRANCE

Abstract

Objectives: We recently introduced a new methodology called quantitative X-ray imaging (qXRI) to investigate bone mineral density in isolated rodent bones. The aims of the present study were to compare DXA and microCT with qXRI in a rat model of disuse osteoporosis. **Methods:** Fourteen Copenhagen rats were injected with a single dose of botulinum toxin (BTX - 2 UI) in the right *Mus quadriceps femoris*. The left hindlimb serves as control. Areal BMD and vBMD were determined with a Hologic Discovery-W device and a Skyscan 1172 microcomputed tomograph (microCT). Absorbing material density (AMD) was determined on digitized X-ray images obtained with a Faxitron M020 device. **Results:** All three methods highlighted significant lower values for aBMD, vBMD and AMD in trabecular and cortical bone in the BTX-injected side. In trabecular bone, aBMD, vBMD and AMD were significantly correlated with BV/TV. In cortical bone, only aBMD and vBMD were significantly correlated with cortical bone mass On the other hand, only AMD was significantly correlated with the mechanical parameters bending strength and bending modulus. **Conclusions:** qXRI is a rapid and cheap method to assess trabecular bone mass in isolated rodent bones and can be used as a surrogate for the densitometry of small animals.

Keywords: Disuse Osteoporosis, qXRI, microCT, Bone Nass, BTX

Introduction

Osteoporosis is a multifactorial disease characterized by a reduction in bone mass associated with an altered bone quality responsible for a loss in mechanical strength of bones leading to increasing risk of fracture[1]. Disuse or prolonged bed rest are recognized conditions associated with a rapid bone loss in humans[2,3]. In order to get a better understanding of the pathophysiology of disuse osteoporosis and the possible use of therapeutic strategies, animal models have been generated[4]. Surgical models, such as amputation and denervation chordotomy lead to a rapid bone loss under the surgical lesion[5]. However, because of confounding factors associated with the surgical trauma, non-surgical techniques are now favored. Among them, hind-limb immobilization by casting (or bandaging) and tail suspension have been widely used[6,7]. We have developed the BTX model using the *Clostridium Botulinum* toxin A to paralyze the *Mus quadriceps femoris* in the rat[8]. A single intra-muscular BTX injection produces reversible skeletal muscle atrophy by blocking the presynaptic release of acetylcholine[9]. The muscle loss becomes appreciable as soon as 1 week post injection and the associated bone reduction can be evidenced by dual energy X-ray absorptiometry (DXA), texture analysis of X-ray images or microcomputed tomogra-

The authors have no conflict of interest.

Corresponding author: Daniel CHAPPARD, M.D., GEROM - LHEA, IRIS-IBS Institut de Biologie en Santé, LUNAM Université Nantes Angers Le Mans CHU d'Angers, 49933 ANGERS Cedex -FRANCE
E-mail: daniel.chappard@univ-angers.fr

Edited by: F. Rauch
Accepted 19 February 2015

phy (microCT) after 3-4 weeks[10,11]. Disuse-associated bone loss is due to a higher expression of resorption genes with a marked decrease in the expression of formation genes[12].

In clinical practice, DXA is the gold standard for assessing bone mass *in vivo*[13]. This methodology consists in measuring the attenuation of two monochromatic X-ray beams (with a high and low energy) by bone and soft tissues. The bone mineral is responsible for X-ray attenuation allowing the measurement of the bone mineral content (BMC). The measure of the bone mineral density (BMD) is derived by normalizing BMC by the area of the 2D bone projection and results into an areal BMD (aBMD). Because of the 2D projection, DXA allows for a global evaluation of the mineral phase of the bone as an organ including the marrow spaces, the vascular channels and the Haversian canals. Furthermore, the PIXImus® device (Lunar, Madison, WI), designed specifically for measuring BMC and BMD in small animals is no longer available and to date no new systems are currently available to measure accurately BMD in mouse and rat.

Another way of exploring bone mass in rodent models is by microCT. In the recent years, improvements have been made in increasing the resolution and now a nominal voxel size of a few micrometers can be obtained with the last generations of microCT devices. However, the X-ray source is usually polychromatic and although filtered, can lead to miscalculation of BMC. With this methodology, the BMC is weighted by the bone volume and leads to a volumetric BMD (vBMD). Recently, a simple and cheap methodology to assess bone mass at the organ level was developed in excised rodent bone, called quantitative X-ray imaging (qXRI)[14]. qXRI is based on single energy X-ray absorption by excised rodent bones in conjunction with an internal standard to estimate the absorbing material density (AMD) and avoid confounding factors such as instability of the X-ray source. We previously reported that qXRI correlated well with bone strength[15,16].

The aims of the present study were to investigate bone microarchitecture and strength by microCT, 3-point bending and quantitative backscattered electron imaging in the BTX rat model. Furthermore, in this rat model of disuse, bone mass was assessed by three different methodologies: DXA, microCT and qXRI. The comparison between these three methodologies and their respective measurement of bone mineral density (aBMD, vBMD and AMD, respectively) were correlated with bone microarchitecture and strength.

Material and methods

Animals

Fourteen Copenhagen male rats weighing 485±37 g were used in this study. Generation of the model has been described in detail elsewhere[8,10]. Briefly, animals received a single injection of BTX (Botox® - Allergan France, 2 IU dissolved in 0.4 mL physiological saline) in the *Mus quadriceps femoris* of the right hindlimb. A 0.4 ml injection of saline was done in the left hindlimb. Paralysis of the right hindlimb was effective as early as 2 days post-injection and last up to 2 months followed by progressive recovery. Animals were sacrificed 28 days post-injection. This procedure was approved by the University of Angers ethical committee (Agreements 49028 and 01732.01) and performed in accordance with the European regulation for the use of animal in experimental procedures.

Quantitative X-ray microradiograph imaging (qXRI)

Digital X-ray images of tibias were recorded in the antero-posterior axis at 18-µm pixel resolution using a Faxitron MX20 device (Edimex, Angers, France) operating with a 2.6X magnification. An aluminum step wedge standard was also imaged in the same conditions. The relative mineral content of calcified tissues was determined as previously reported[15,16] with several modifications. Briefly, a 3-mm thick steel plate and a 3-mm thick poly (methylmethacrylate) plate were used on each radiograph and served as internal standards for calibration of the gray level. X-rays images were recorded at 26kV/300 µA with a monochromatic X-ray beam (beryllium-filtered tungsten Lα radiation with a wavelength of 14.7 nm). At this wavelength, the mass coefficient of apatite is about 10 times that of water or protein and as such the X-ray absorption is mainly caused by the mineral component[17]. Before converting the 16-bit DICOM images into 8-bit tif images, the histogram was equalized from the plastic (gray level 0) to the steel (gray level 255) standards using a lab-made routine in ImageJ 1.45s (NIH, Bethesda, MD)[18]. Analysis was performed either in the proximal metaphysis, using the growth plate at a upper limit, or in the center of the diaphysis by overimposing a region of interest (ROI -square, 4 mm side). The frequency of occurrence of an *i* gray level (*Fi*) in the ROI was calculated as follows:

$$F_i = 100 \times \frac{N_i}{N_t}$$

Where *Ni* represents the number of pixels with the *i* gray level and *Nt* the total number of pixels. The frequency distribution of gray level was plotted and the mean gray level (GL_{mean}) of each bone was deduced from this distribution using the following formula:

$$GL_{mean} = \sum \frac{F_i \times GLi}{100}$$

where *GLi* represents the value of the i gray level. Figure 1 represents examples of GL_{mean} calculation.

The bone outer diameter (B.Dm) in the antero-posterior axis was determined with a digital caliper at the measurement site. B.Dm and gray levels of the aluminum step wedge standard were used to convert GL_{mean} into the absorbing material density (AMD) in a similar way as reported by Boivin and Meunier[17]. Increasing gradations of mineralization density were represented in 16 equal intervals using the 16-colours lookup table in ImageJ.

X-ray microcomputed tomography

MicroCT analysis was performed on tibias with a Skyscan 1172 microtomograph (Bruker-Skyscan, Kontich, Belgium) equipped with an X-ray tube working at 69 kV/100 µA. An

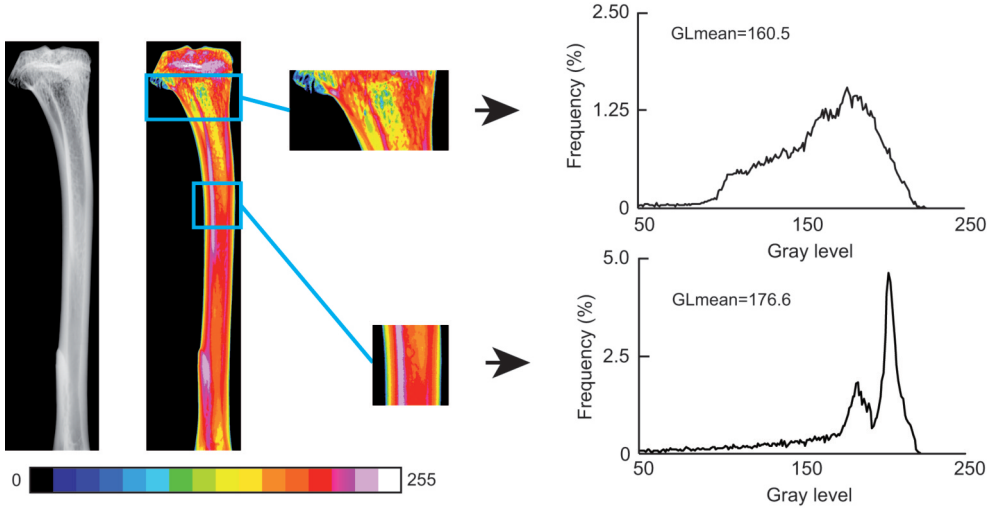

Figure 1. Examples of qXRI assessment. A standardized X-ray was taken and the gray level was adjusted to the plastic and steel standards. Then the trabecular and cortical ROI were overimposed and the corresponding area was selected. To allow a visual characterization of the gray level distribution, a 16 color look-up table was applied. The frequency distribution of each gray level was plotted and the mean gray level determined. Then the GL_{mean} was converted into AMD by using the aluminum step wedge standard.

isotropic voxel size was fixed at 13.4 µm, the rotation step at 0.25° and exposure was performed with a 0.5 mm aluminum filter. Volumetric bone mineral density (vBMD) measurements were performed according to the manufacturer recommendations by using calibrated phantoms adapted to rat bones[19]. The CTAn Software (Skyscan, release 1.10.1.0) was used to measure the bone mass of the tibia (upper metaphysis). The first image selected for analysis was located just under the growth plate and then extended on 300 sections in the tibia. The volume of interest (VOI) was designed by interactively drawing a polygon on each 2D section. Only a few number of polygons need to be drawn (e.g. on the first section, several at the middle, and on the final section) since a routine facility calculated all the intermediary masks by interpolation. A first VOI (located at the same bone regions than qXRI) containing only trabecular bone and marrow cavity was drawn and a global threshold was used to select the trabeculae[20]. The trabecular bone volume (BV/TV, in %) representing the percentage of the cancellous space occupied by trabecular bone was determined. This VOI was also used to measure the trabecular vBMD (in g/cm^3). Another VOI comprising only cortical bone was obtained at the midshaft of each bone to determine cortical vBMD. The following microarchitectural descriptors of cortical bone: cortical thickness (Ct.Th, in µm), cortical area (Ct.Ar, in mm^2) and cross-sectional moment of inertia (CSMI, in mm^4) were measured with a lab-based routine made with ImageJ according to guidelines and nomenclature proposed by the American Society for Bone and Mineral Research[21].

Dual energy X-ray absorptiometry (DXA)

Ex vivo DXA scans were performed with a Hologic discovery W (Hologic Inc, Bedfor, MA) using the APEX software in the high resolution small animal setting (release 3.3, Hologic Inc). Tibias were placed in a plastic jar filled with water (1 cm thickness) and with a mask drawn at the bottom to ensure reproducible positioning of bones. The densitometer was operated at 140/100 kV with a pixel resolution of 700 µm. The proximal metaphysis was used to evaluate trabecular bone by selecting a ROI up to 4mm from the growth plate. The midshaft tibia was used to measure cortical bone by applying a 4-mm ROI at the center.

Three-point bending

Three-point bending experiments were performed on the tibias. Before mechanical testing, bones were rehydrated in saline for 24 hrs at room temperature as described elsewhere[22]. Three-point bending strength was measured with a constant span length of 20 mm. The press head as well as the two support points were rounded to avoid shear load and cutting. Bones were positioned horizontally with the anterior surface facing upward, centered on the support and the pressing force was applied vertically to the midshaft of the bone. Each bone was tested with a loading speed of 2 mm/min^{-1} until failure with a 500N load cell on an Instron 5942 device (Instron, Elancourt, France). The load-time curve obtained was converted into a load-displacement curve by the Bluehill 3 software (Instron). Ultimate load and ultimate displacement were respectively defined as the maximum load and maximum displacement recorded before breakdown of the bone. Stiffness was calculated as the slope of the elastic deformation of the bone. The total absorbed energy was defined as the total area under the load-displacement curve and represented the total energy absorbed by the midshaft femur. Intrinsic parameters were calculated according to previous published equations[23,24].

	Saline-injected	BTX-injected	P value
BV/TV (%)	49.5 ± 0.8	41.2 ± 0.7	<0.001
B.Dm (mm)	3.2 ± 0.1	3.2 ± 0.1	NS
Ma.Dm (mm)	2.0 ± 0.1	2.1 ± 0.1	NS
Ct.Ar (mm^2)	5.4 ± 0.1	5.2 ± 0.1	<0.05
Ct.Th (μm)	592 ± 8	560 ± 5	<0.01
CSMI (mm^4)	4.2 ± 0.2	4.4 ± 0.2	NS

Table 1. Bone micro-architectural parameters. Analyses were performed on trabecular and cortical bone in saline-injected (left hindlimb) and BTX-injected (right hindlimb) tibias. (NS= non-significant).

	Saline-injected	BTX-injected	P value
Ultimate load (N)	92.8 ± 3.4	91.2 ± 2.2	NS
Ultimate displacement (mm)	0.7 ± 0.01	0.6 ± 0.01	NS
Stiffness (N/mm)	221.1 ± 6.0	214.9 ± 7.3	NS
Absorbed Energy (N.mm)	36.8 ± 2.8	31.3 ± 2.6	NS
Bending stress (MPa)	173.4 ± 4.7	172.9 ± 5.7	NS
Ultimate strain	0.03 ± 0.001	0.03 ± 0.001	NS
Bending modulus (GPa)	8.9 ± 0.4	8.4 ± 0.3	NS
Work to fracture (kJ/m^2)	4.7 ± 0.3	3.8 ± 0.3	<0.05
Ca_{peak} (%)	26.2 ± 0.2	24.9 ± 0.3	<0.05
Ca_{mean} (%)	25.7 ± 0.2	24.4 ± 0.3	<0.05
Ca_{width} (%)	3.2 ± 0.01	3.2 ± 0.01	NS
MCM (mm^2)	5.7 ± 0.1	4.9 ± 0.1	<0.001

Table 2. Mechanical response and matrix properties of cortical bone. (NS= non-significant).

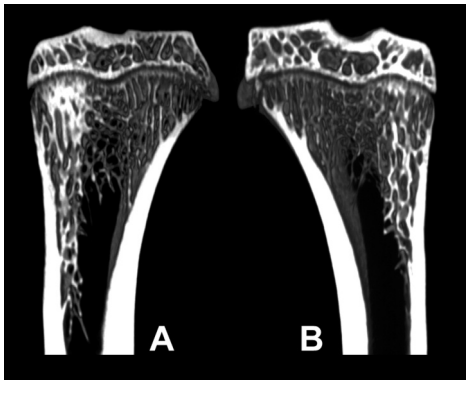

Figure 2. MicroCT of the tibiae of the same rat. A) BTX injected side (right), B) saline injected side (left). 3D reconstruction with a volume rendering algorithm.

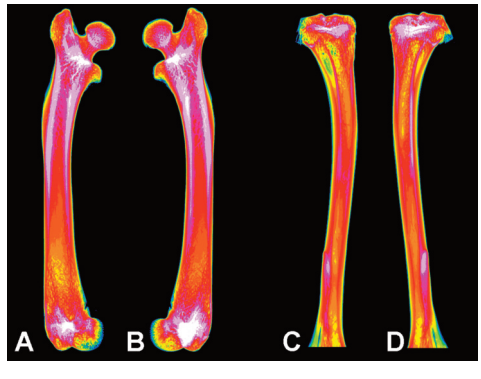

Figure 3. Quantitative X-ray imaging of the femurs and tibiae of the same rat. A and C) BTX injected side (right), B and D) saline injected side (left). The changes are obvious at the lower metaphysis of the femur and at the upper metaphysis of the tibia.

Quantitative backscattered electron imaging (qBEI)

Quantitative backscattered electron imaging was employed to determine the bone mineral density distribution (BMDD) in tibia cortical bone as previously reported[25,26]. This methodology has been described in full details elsewhere[26]. After 3-point bending, the upper tibia extremities were embedded undecalcified in poly (methylmethacrylate). Blocks were polished to a 0.5-μm finish with diamond particles, carbon-coated and observed with a scanning electron microscope (EVO LS10, Carl Zeiss Ltd, Nanterre, France) equipped with a five quadrants

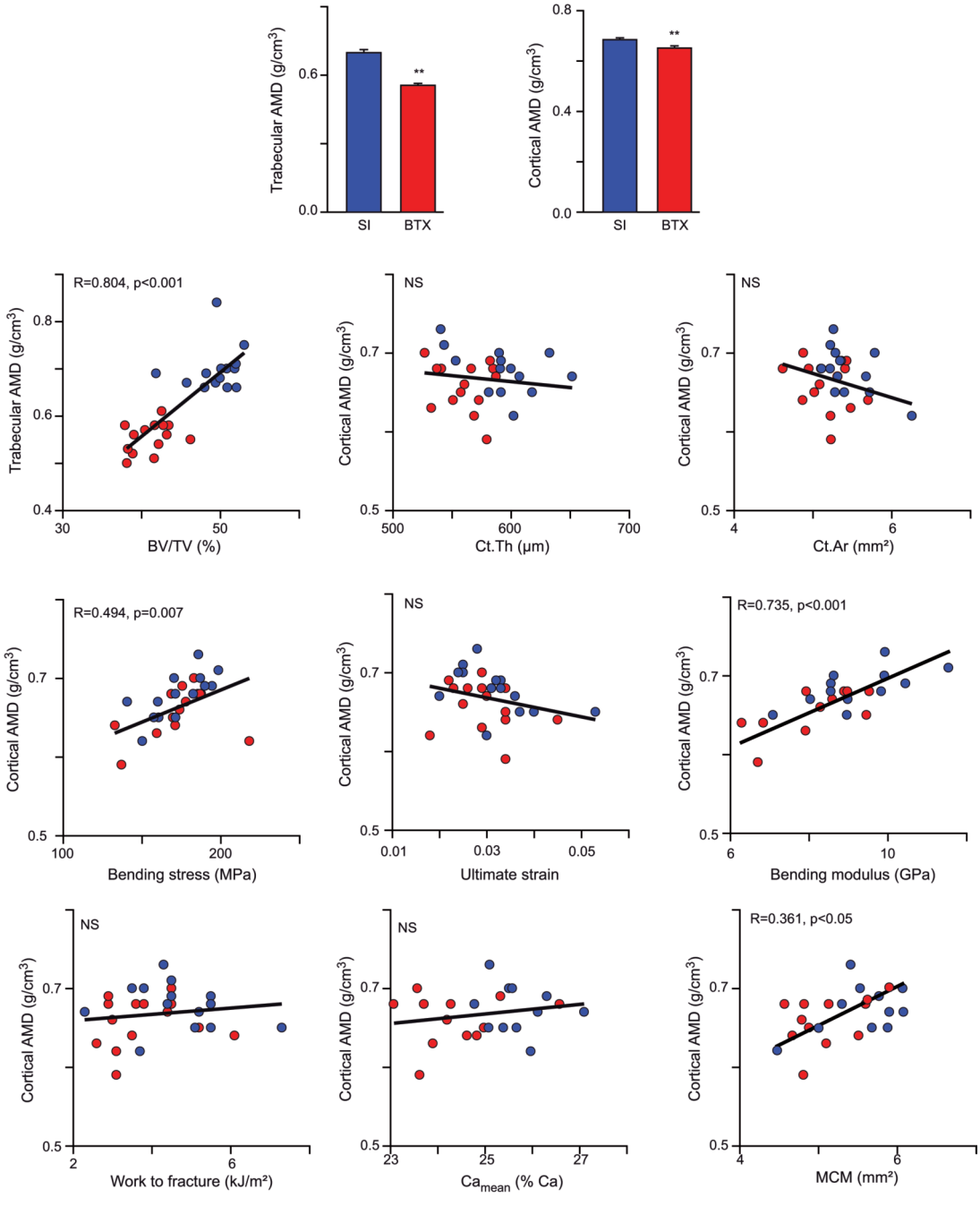

Figure 4. Quantitative X-ray imaging and correlation with microarchitectural and biomechanical parameters. (A) Trabecular and (B) cortical absorbing material density (AMD) in non- and BTX-injected side. Both parameters were significantly lower in the BTX-treated side. **: p<0.01 vs. saline-injected side. Regression analyses between (C) trabecular AMD and trabecular bone volume (BV/TV), cortical AMD and (D) cortical area, (E) cortical thickness, (F) bending stress, (G) ultimate strain, (H) bending modulus, (I) work to fracture, (J) Ca_{mean} and (K) MCM. Color code: blue= saline-injected side and red= BTX-injected side; NS= non-significant.

semi-conductor backscattered electron detector. The microscope was operated at 20 keV with a probe current of 250 pA and a working distance of 15 mm. The cortical bone area located at the mid-diaphysis was imaged at a 100X nominal magnification, corresponding to a pixel size of 1 µm per pixel. Six images per samples were taken and the gray levels distribution of each image was analyzed with a lab-made routine in ImageJ. Three variables were obtained from the bone mineral density distribution: Ca_{peak} as the most frequently observed calcium concentration, Ca_{mean} as the average calcium concentration and Ca_{width} as the width of the histogram at half maximum of the peak. The mineralized cortical mass (MCM) was calcu-

lated in order to account for modification in the degree of mineralization and cortical mass. This parameter for a given *i* animal was calculated as follow:

$$MCM\ (i) = \frac{Ct.Ar\ (i) \times Ca_{mean}\ (i)}{Ca_{mean\text{-}group}}$$

where *Ct.Ar(i)* is the cortical area of the *i* animal, Ca_{mean} *(i)* is the mean calcium concentration of the *i* animal and $Ca_{mean\text{-}group}$ the mean calcium concentration of all animals from the right (BTX-injected) or left (saline-injected) hindlimb group.

Statistical analysis

Statistical analysis was performed using the Systat statistical software release 13.0 (Systat Software Inc., San José, CA). All data were expressed as mean±standard error of the mean (SEM). Differences between groups were analyzed by a non-parametric Kruskal-Wallis test. Differences were considered significant when $p<0.05$.

Results

Assessment of bone microarchitecture, mechanical response and mineralization properties in the BTX rat

In order to ensure that BTX injections led to deteriorations of trabecular microarchitecture, we assessed trabecular parameters by microCT (Figure 2). As reported Table 1, BTX-injected sides presented with a significant 17% reduction in BV/TV as compared with saline-injected sides ($p<0.001$). Cortical bone microarchitecture was also investigated and a significant but moderate reductions were evidenced in Ct.Ar (-5.1%) and Ct.Th (-5.4%) in the BTX-injected hindlimb ($p=0.04$ and $p=0.003$, respectively). None of the other cortical parameters were significantly altered in BTX-injected hindlimb.

Mechanical response of the cortical bone was assessed at the midshaft tibia by 3-point bending. As reported Table 2, only a significant reduction in the work to fracture (-19%) was observed in BTX-injected hindlimb as compared to the saline-injected side. None of the other parameters (extrinsic and intrinsic) were significantly different between the two sides. Furthermore, the bone mineral density distribution was altered in the BTX-injected side with significant reductions in Ca_{peak} and Ca_{mean} by 5% and 5%, respectively.

Assessment of bone mineral density by qXRI, DXA and microCT

qXRI

The absorbing material density (AMD) was determined at the proximal tibia metaphysis (trabecular AMD) and tibia midshaft (cortical AMD). The aspect of the femur and tibia of a BTX rat appear on Figure 3. Quantitative results are depicted on Figure 4A and 4B. Trabecular and cortical AMDs were significantly lower by 20.6% and 4.8% in the BTX-injected as compared with the saline-injected side ($p<0.001$ and $p=0.007$, respectively). A good correlation between trabecular AMD and BV/TV was observed ($R=0.804$, $p<0.001$). On the other hand, cortical AMD was not correlated with neither Ct.Ar nor Ct.Th. Cortical AMD was linked to mechanical properties with significant correlations with bending stress ($R=0.494$, $p=0.007$) and bending modulus ($R=0.735$, $p<0.001$). On the other hand, no correlations were evidenced between cortical AMD and ultimate stress, work to fracture and Ca_{mean}.

However as the cortical bone mass and degree of mineralization were altered in the BTX-injected site, we assessed whether cortical AMD could be linked to MCM, a parameter accounting for cortical area and degree of mineralization with qBEI (Figure 5). And indeed, cortical AMD was significantly associated with MCM ($R=0.361$, $p<0.05$).

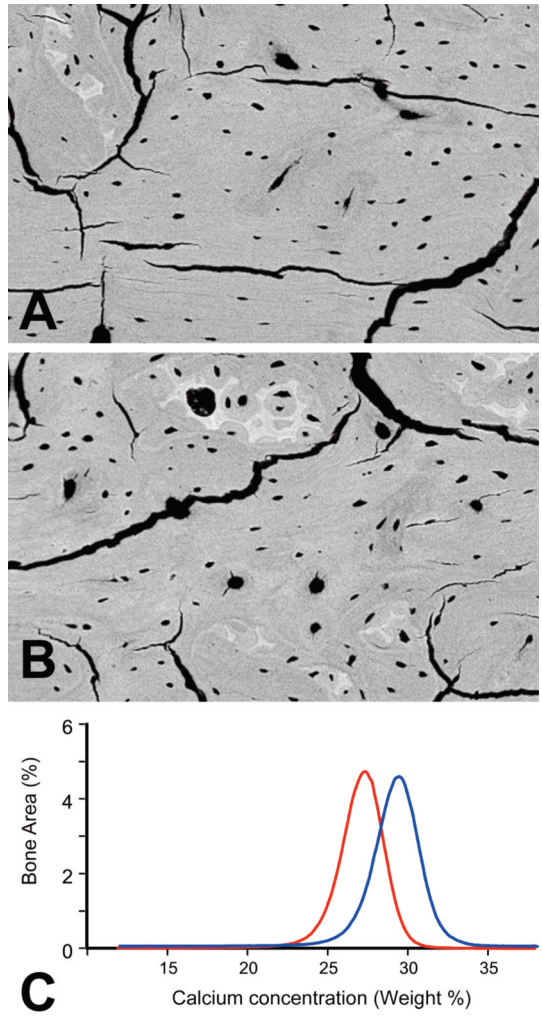

Figure 5. Mineralization degree determined on BSE images obtained by scanning electron microcopy of the tibias from the same rat, original magnification x200. The cracks occur when the blocks are placed under vacuum in the SEM. A) BTX injected side (right), B) saline injected side (left), C) frequency distribution of the grey level in the two groups: blue= saline-injected side and red= BTX-injected side.

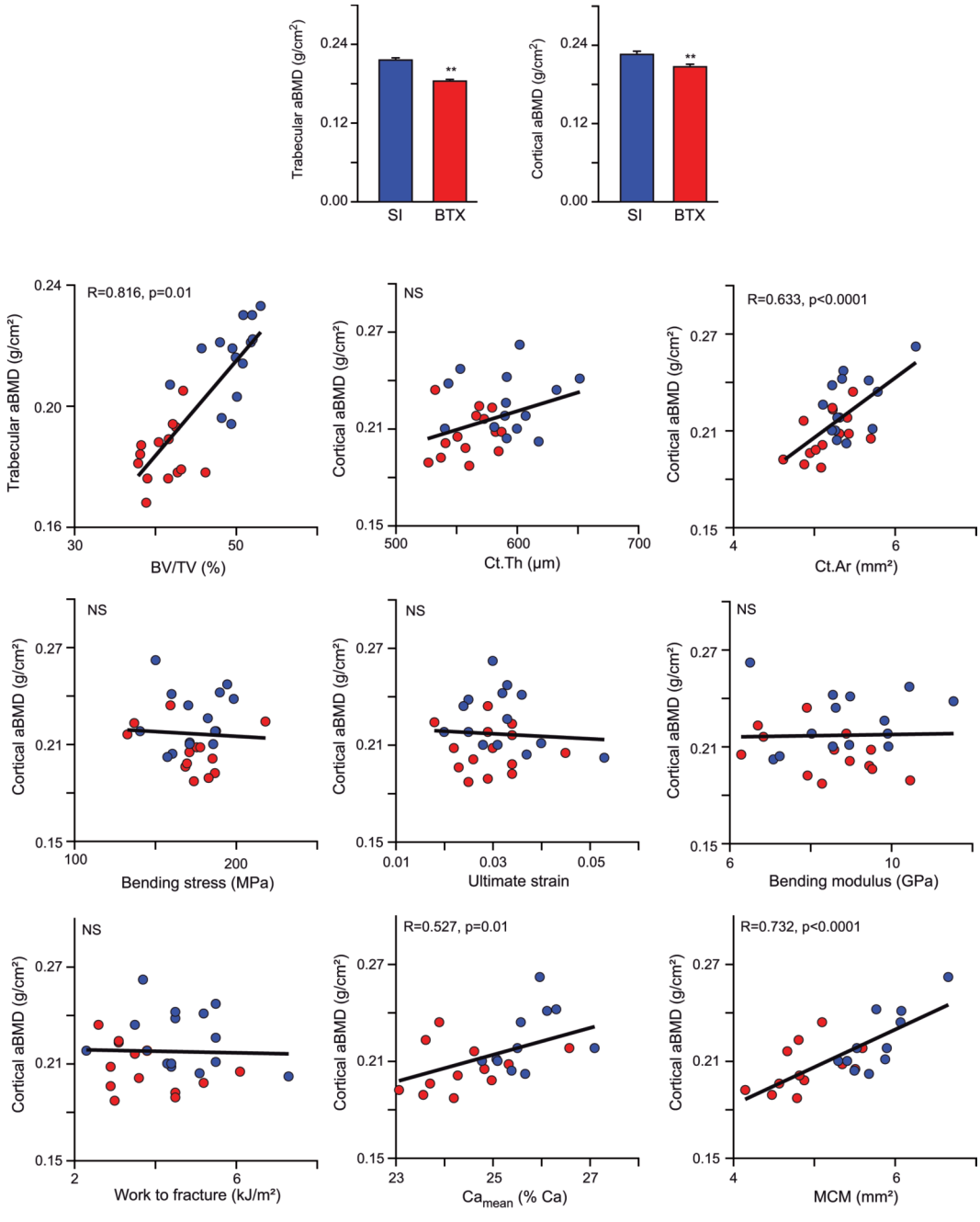

Figure 6. Bone mineral density assessed by dual-energy X-ray absorptiometry and correlation with microarchitectural and mechanical parameters. (A) Trabecular and (B) cortical bone mineral density (aBMD) in non- and BTX-injected side. Both parameters were significantly lower in the BTX-treated side. **: p<0.01 vs saline-injected side. Regression analyses between (C) trabecular aBMD and BV/TV, cortical aBMD and (D) cortical area, (E) cortical thickness, (F) bending stress, (G) ultimate strain, (H) bending modulus, (I) work to fracture, (J) Camean and (K) MCM. Color code: blue= saline-injected side and red= BTX-injected side; NS= non-significant.

DXA

Trabecular and cortical aBMD were determined at the proximal tibia metaphysis (trabecular) and tibia midshaft (cortical) (Figure 6). Trabecular aBMD was significantly reduced by 18% in the BTX-injected side as compared to the other hindlimb (p<0.001). At the cortical site, aBMD was significantly reduced by 8.9% in the BTX-injected side (p=0.007). Trabecular aBMD was significantly correlated with BV/TV (R=0.816, p=0.01). Cortical aBMD was significantly correlated with Ct.Ar (R=0.633, p<0.001), Ca_{mean} (R=0.527, p=0.01) and MCM (R=0.732, p<0.001). On the other hand, no significant correlations were found between cortical aBMD and the other investigated parameters, especially mechanical parameters.

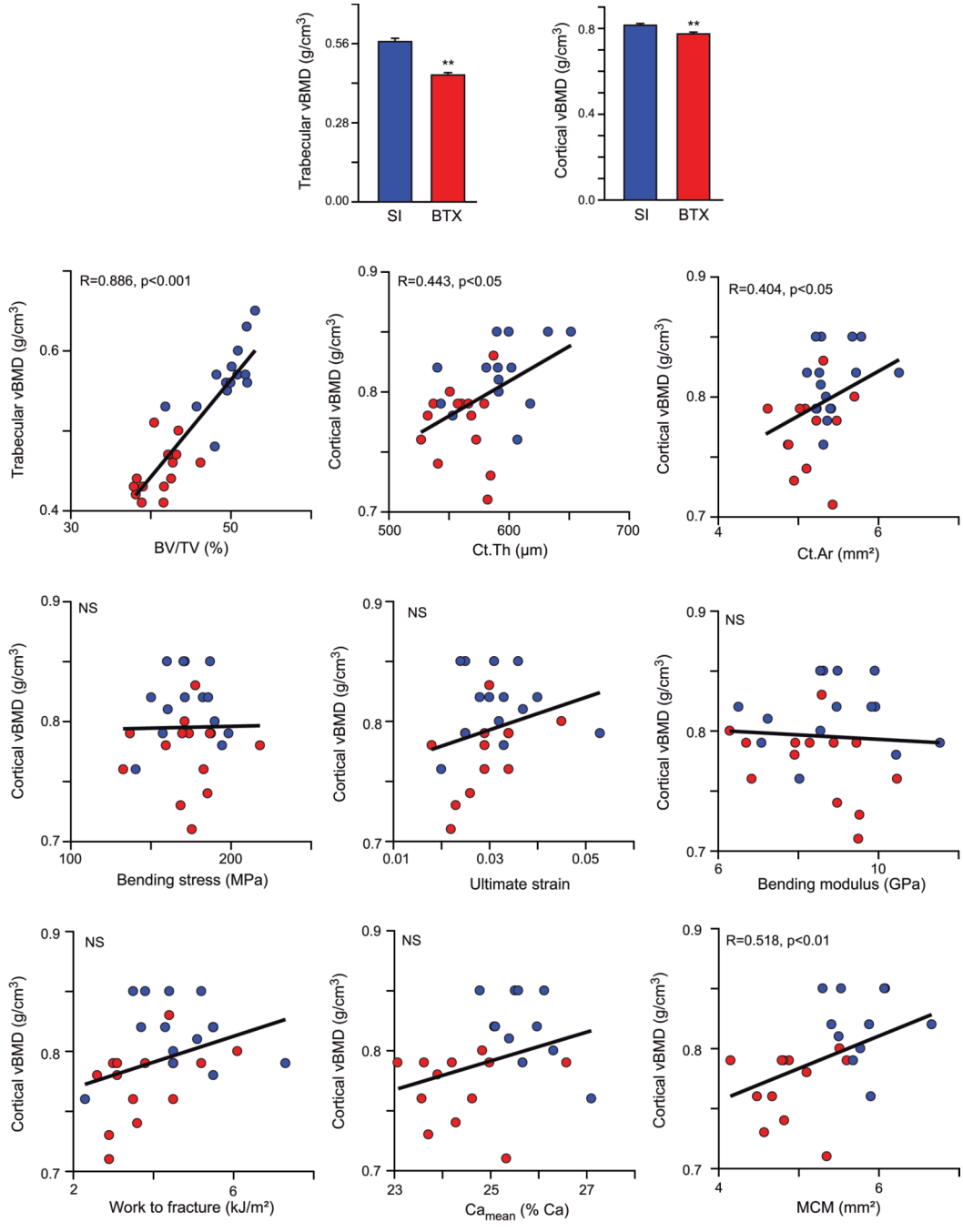

Figure 7. Bone mineral density assessed by microCT and correlation with microarchitectural and mechanical parameters. (A) Trabecular and (B) cortical bone mineral density (vBMD) in non- and BTX-injected side. Both parameters were significantly lower in the BTX-treated side. **: p<0.01 vs saline-injected side. Regression analyses between (C) trabecular vBMD and BV/TV, cortical vBMD and (D) cortical area, (E) cortical thickness, (F) bending stress, (G) ultimate strain, (H) bending modulus, (I) work to fracture, (J) Ca_{mean} and (K) MCM. Color code: blue= saline-injected side and red= BTX-injected side; NS= non-significant.

MicroCT densitometry

Trabecular and cortical vBMDs were significantly lowered by 21% and 4.9%, respectively in BTX- as compared with saline-injected sides (p<0.001 and p=0.003, respectively) (Figure 7). Trabecular vBMD was significantly correlated with BV/TV (R=0.886, p<0.001). Cortical vBMD was found associated to Ct.Th (R=0.443, p=0.02), Ct.Ar (R=0.404, p=0.03) and MCM (R=0.518, p=0.01). None of the other investigated parameters including mechanical parameters was significantly correlated to cortical vBMD.

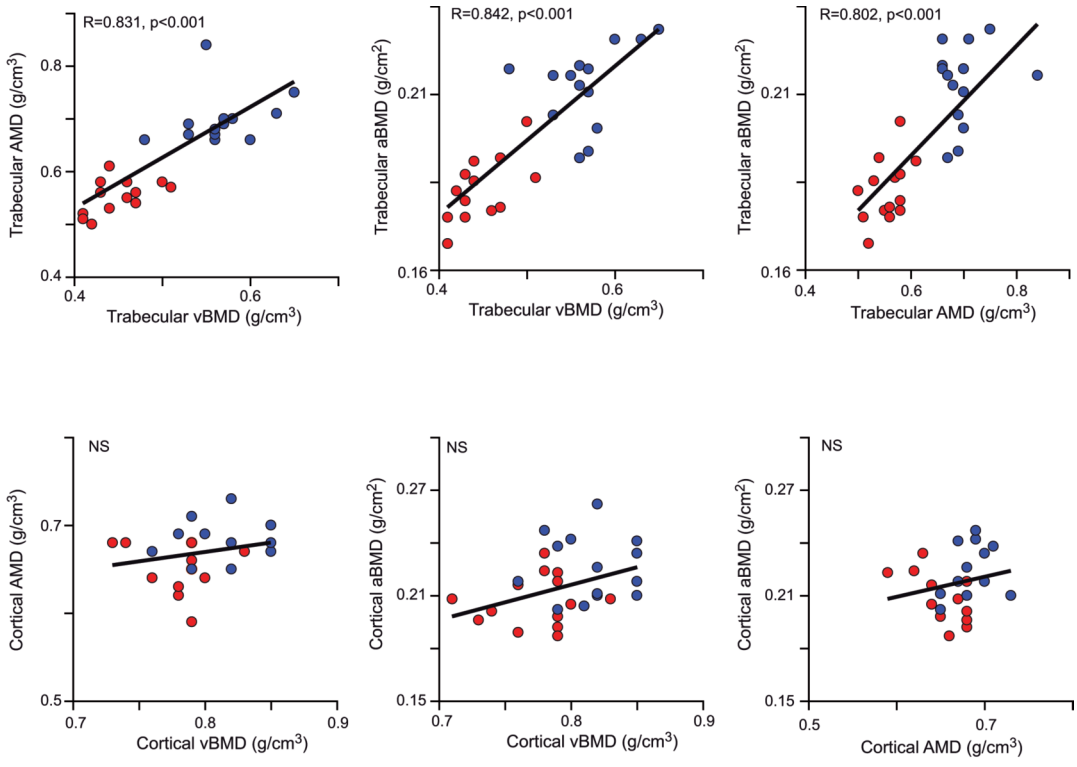

Figure 8. Correlation between AMD, aBMD and vBMD in (A) trabecular and (B) cortical compartment. Color code: blue = saline-injected side and red = BTX-injected side; NS = non-significant.

Trabecular AMD was significantly correlated with trabecular BMD, BMC and vBMD

Trabecular AMD was significantly correlated with trabecular aBMD (R=0.802, p<0.001) and trabecular vBMD (R=0.842, p<0.001) (Figure 8). On the other hand, no correlations were found between cortical AMD, cortical aBMD and cortical vBMD.

Discussion

Osteoporosis is a disease characterized by alterations of bone mass and quality leading to an increase risk of bone fracture. Different factors can result in osteoporosis and among them disuse is recognized as a contributing factor leading to a rapid bone loss in human and animals[27].

In the present study, we used a validated model of disuse-osteoporosis caused by the injection of *Botulinum* toxin and a subsequent paralysis of the *Mus quadriceps femoris*. This model has been fully characterized previously by us and other groups in term of bone microarchitecture[8,10-12, 28-32]. Here we report, as expected, significant alterations of trabecular and cortical bone masses (-17% in BV/TV, -5.1% in Ct.Ar and -5.4% in Ct.Th).

Unexpectedly, despite these alterations in cortical microarchitecture, the mechanical resistance of cortical bone as assessed by 3-point bending was only moderately reduced in the BTX-injected hindlimb and only a lower work to fracture was evidenced. These findings are in agreement with the observations of Sheng et al. or more recently Grubbe et al.[33,34]. Indeed, these authors reported, using Sprague Dawley or Wistar rats, that the mechanical resistance of BTX animal was only moderately affected at mid-diaphysis with a significant reduction in ultimate load. In the present study, we observed a significant reduction in the work to fracture which, as defined by Ritchie et al, is a measure of bone toughness[23]. However, very little was known about the quality of the bone matrix in their animal model and as such in order to ascertain whether the mineralization was hampered, we evaluated the bone mineral density distribution by qBEI. We evidenced a significant reduction in the mean and peak calcium concentrations by 5%, that could potentially be responsible for the reduction in work to fracture as reported above although the mechanisms leading to such observation have yet to be determined.

Another aim of this study was to determine whether qXRI could be a validated method to highlight change in trabecular and cortical bone masses in rats and how it performs compared to DXA and high-resolution microCT. All these three methodologies are based on the absorption of X-rays by the bone mineral. As expected, trabecular AMD, aBMD and vBMD were significantly reduced in the BTX-injected side in the same order of magnitude. Additionally, all three parameters correlated well with BV/TV (R>0.8). On the other hand, cortical AMD failed to correlate with cortical microarchitecture whilst

cortical aBMD and vBMD did. Surprisingly, cortical AMD and vBMD failed to correlate with the mean calcium concentration (Ca_{mean}) whilst aBMD did. However, all three parameters were correlated with the Mineralized Cortical Mass, a parameter introduced in this study to account for reduction in cortical bone mass and mineralization of this envelope. It is worth noting that the order of correlation with MCM was aBMD>vBMD>AMD.

As said above, the three methodologies are based on the absorption of an incident X-ray beam by the bone mineral. However, the energy of the X-ray beam is different between the three methodologies as X-rays were generated at different accelerating voltage. Indeed, it is with DXA that X-rays were the most energetic followed by microCT and finally qXRI. This is important as high energy X-rays are less absorbed by soft material such as skin, muscle or even bone marrow and are high enough not to be totally absorbed by the bone mineral. The low accelerating voltage used for qXRI makes this methodology useable only in small animal models such as mouse or rat models.

An intriguing result was that only cortical AMD correlated with several 3-point bending parameters. The assumption that qXRI correlated well with mechanical resistance of the bone had been postulated before by Bassett et al.[35]. However, at this point, we do not have explanation to understand the failure of aBMD and vBMD to correlate with mechanical parameters.

qXRI was also performed by other research groups, but the way results are reported are slightly different although the experimental setups are very similar[14-16,35]. However, although these authors used a similar setup to perform qXRI, the interpretation of the data is either made by comparing cumulative frequency histogram[14,35] or calculating a mean gray level[15,16]. In the present study, we have improved the detection method by taking into account the length of the bone tissue crossed by the X-ray beam. This allowed us to convert the mean gray level into the absorbing material density expressed in g/cm^3 of material. It was not the case with the BTX model, but it is important to take into account the length of the bone crossed by the X-ray beam in situations where the outer bone diameter is affected.

In conclusion, bone quality is altered in the BTX- model of disuse at the microarchitecture level but also in the mineral component of the bone matrix. Furthermore, qXRI and the resulting AMD appeared informative in term of trabecular bone and compared very well to other validated methodologies such as DXA and microCT. However, although qXRI may present several limitations in the assessment of cortical bone mass, this methodology correlated well with mechanical parameters.

Acknowledgements

This work was made possible by grants from Contrat Region Pays de la Loire: Bioregos2 program.

References

1. Anonymous. Consensus development conference. Prophylaxis and treatment of osteoporosis. Am J Med 1993; 94:646-50.
2. Minaire P, Neunier P, Edouard C, Bernard J, Courpron P, and Bourret J. Quantitative histological data on disuse osteoporosis: comparison with biological data. Calcif Tissue Res 1974;17:57-73.
3. Krølner B, and Toft B. Vertebral bone loss: an unheeded side effect of therapeutic bed rest. Clin Sci 1983;64:537-40.
4. Jee WS, and Ma Y. Animal models of immobilization osteopenia. Morphologie 1999;83:25-34.
5. Jiang SD, Jiang LS, and Dai LY. Effects of spinal cord injury on osteoblastogenesis, osteoclastogenesis and gene expression profiling in osteoblasts in young rats. Osteoporos Int 2007;18:339-49.
6. Wronski TJ, and Morey-Holton ER. Skeletal response to simulated weightlessness: a comparison of suspension techniques. Aviat Space Environ Med 1987;58:63-8.
7. Milstead JR, Simske SJ, and Bateman TA. Spaceflight and hindlimb suspension disuse models in mice. Biomed Sci Instrum 2004;40:105-10.
8. Chappard D, Chennebault A, Moreau M, Legrand E, Audran M, and Basle MF. Texture analysis of X-ray radiographs is a more reliable descriptor of bone loss than mineral content in a rat model of localized disuse induced by the Clostridium botulinum toxin. Bone 2001;28:72-9.
9. Dickerson TJ, and Janda KD. The use of small molecules to investigate molecular mechanisms and therapeutic targets for treatment of botulinum neurotoxin A intoxication. ACS Chem Biol 2006;1:359-69.
10. Blouin S, Gallois Y, Moreau MF, Baslé MF, and Chappard D. Disuse and orchidectomy have additional effects on bone loss in the aged male rat. Osteoporos Int 2007; 18:85-92.
11. Thomsen JS, Christensen LL, Vegger JB, Nyengaard JR, and Bruel A. Loss of bone strength is dependent on skeletal site in disuse osteoporosis in rats. Calcif Tissue Int 2012;90:294-306.
12. Marchand-Libouban H, Le Drevo MA, and Chappard D. Disuse induced by botulinum toxin affects the bone marrow expression profile of bone genes leading to a rapid bone loss. J Musculoskelet Neuronal Interact 2013;13:27-36.
13. Blake GM, and Fogelman I. The clinical role of dual energy X-ray absorptiometry. Eur J Radiol 2009;71:406-14.
14. Bassett JH, van der Spek A, Gogakos A, and Williams GR. Quantitative X-ray imaging of rodent bone by Faxitron. Meth Mol Biol 2012;816:499-506.
15. Mabilleau G, Mieczkowska A, Irwin N, Flatt PR, and Chappard D. Optimal bone mechanical and material properties require a functional glucagon-like peptide-1 receptor. J Endocrinol 2013;219:59-68.
16. Mieczkowska A, Irwin N, Flatt PR, Chappard D, and Mabilleau G. Glucose-dependent insulinotropic polypeptide (GIP) receptor deletion leads to reduced bone strength and quality. Bone 2013;56:337-42.
17. Boivin G, and Meunier PJ. The degree of mineralization of bone tissue measured by computerized quantitative contact microradiography. Calcif Tissue Int 2002;70:503-11.

18. Rasband WS ImageJ, http://imagej.nih.gov/ij/, . In: U. S. National Institutes of Health (ed.). Bethesda, Maryland, USA; 1997-2014.
19. Anonymous Bone mineral density (BMD) and tissue mineral density (TMD) calibration and measurement by micro micro micro-CT using Bruker-MicroCT- Analyser, pp. 1-30: Bruker MicroCT; 2012.
20. Tassani S, Korfiatis V, and Matsopoulos G. Influence of segmentation on micro-CT images of trabecular bone. J Microsc 2014;256:75-81.
21. Dempster DW, Compston JE, Drezner MK, Glorieux FH, Kanis JA, Malluche H, et al. Standardized nomenclature, symbols, and units for bone histomorphometry: a 2012 update of the report of the ASBMR Histomorphometry Nomenclature Committee. J Bone Miner Res 2013;28:2-17.
22. Ammann P, Badoud I, Barraud S, Dayer R, and Rizzoli R. Strontium ranelate treatment improves trabecular and cortical intrinsic bone tissue quality, a determinant of bone strength. J Bone Miner Res 2007;22:1419-25.
23. Ritchie RO, Koester KJ, Ionova S, Yao W, Lane NE, Ager JW, 3rd. Measurement of the toughness of bone: a tutorial with special reference to small animal studies. Bone 2008;43:798-812.
24. Turner CH, and Burr DB. Basic biomechanical measurements of bone: a tutorial. Bone 1993;14:595-608.
25. Gaudin-Audrain C, Irwin N, Mansur S, Flatt PR, Thorens B, Basle M, et al. Glucose- dependent insulinotropic polypeptide receptor deficiency leads to modifications of trabecular bone volume and quality in mice. Bone 2013; 53:221-30.
26. Roschger P, Fratzl P, Eschberger J, Klaushofer K. Validation of quantitative backscattered electron imaging for the measurement of mineral density distribution in human bone biopsies. Bone 1998;23:319-26.
27. Bikle DD, Sakata T, Halloran BP. The impact of skeletal unloading on bone formation. Gravit Space Biol Bull 2003;16:45-54.
28. Manske SL, Boyd SK, Zernicke RF. Muscle and bone follow similar temporal patterns of recovery from muscle-induced disuse due to botulinum toxin injection. Bone 2010;46:24-31.
29. Libouban H, Blouin S, Moreau MF, Baslé MF, Audran M, and Chappard D. Effects of risedronate in a rat model of osteopenia due to orchidectomy and disuse: densitometric, histomorphometric and microtomographic studies. Micron 2008;39:998-1007.
30. Ellman R, Grasso DJ, van Vliet M, Brooks DJ, Spatz JM, Conlon C, et al. Combined effects of botulinum toxin injection and hind limb unloading on bone and muscle. Calcif Tissue Int 2014;94:327-37.
31. Aydin A, Memisoglu K, Cengiz A, Atmaca H, Muezzinoglu B, and Muezzinoglu US. Effects of botulinum toxin A on fracture healing in rats: an experimental study. J Orthop Sci 2012;17:796-801.
32. Atmaca H, Aydin A, and Musaoglu R. Experimental model of osteoporosis: comparison between ovariectomy and botulinum toxin a. Acta Ortop Bras 2013;21:340-3.
33. Grubbe MC, Thomsen JS, Nyengaard JR, Duruox M, and Bruel A. Growth hormone mitigates loss of periosteal bone formation and muscle mass in disuse osteopenic rats. J Musculoskelet Neuronal Interact 2014;14:473-83.
34. Sheng ZF, Ma YL, Tong D, Fang DY, Liang QC, Liu LH, et al. Strontium ranelate prevents bone loss in a rat model of localized muscle paralysis. Ann Biomed Eng 2012; 40:657-65.
35. Bassett JH, Gogakos A, White JK, Evans H, Jacques RM, van der Spek AH, et al. Rapid-throughput skeletal phenotyping of 100 knockout mice identifies 9 new genes that determine bone strength. PLoS Genet 2012; 8:e1002858.